A Dispersive Quadruplet Structure for Monoblock Dielectric Resonator Filters

Yan Zhang, Yuliang Chen, *Graduate Student Member, IEEE*, and Ke-Li Wu, *Fellow, IEEE*

***Abstract*— In this article, a dispersive quadruplet structure that can flexibly control the rejection response of a high-Q monoblock dielectric resonator (MDR) filter using a shared cavity is introduced. Being simple in structure, traditional partitioning walls for positive couplings are replaced by metalized through holes. The dispersion effect of the blind hole for negative coupling can be effectively compensated by parasitic cross couplings by appropriately managing the through holes, leading to a shared rectangular cavity for the resonators. With the aggregated effort of the blind hole and through holes, the rejection response can be well controlled to a certain extent. The closed-form mathematic transformation from the dispersion-less to dispersive coupling matrices of the quadruplet is also given for explaining the working principle of the dispersive quadruplet and providing a design guideline. Two design examples are presented: a quadruplet MDR filter with two symmetric transmission zeros (TZs); and an eight-pole MDR filter consisting of a proposed quadruplet and a box unit, showing superior performance of the MDR quadruplet structure in realizing a wide range of rejection responses and validating the theory for practical applications. The experimental result demonstrates that the MDR quadruplet is particularly useful when rejection specifications near the passband are stringent.**

***Index Terms*— Cross coupling, dispersive coupling, monoblock dielectric resonator (MDR) filter, quadruplet block, transmission zeros (TZs).**

I. Introduction

TRANSMISSION zeros (TZs) play an essential role in realizing high rejection roll-off in microwave bandpass filters. Traditionally, cross couplings between two nonadjacent resonators [1] and extracted-pole sections [2] are popularly used to generate TZs. With cross couplings, a signal on the main path is split into multiple paths and then recombined at another node. One or more TZs may occur at the frequencies at which the recombined signals interfere with each other. The extracted-pole section uses a different mechanism, with which a dangling resonator joined at a nonresonant node is introduced to create short-circuiting on the main path at a designated frequency, leading to a TZ.

Monoblock dielectric resonator (MDR) filters have regained their popularity in the wireless industry for the fifth-generation (5G) wireless systems recently. Tracing back to the 1980s, MDR filter was first built in the comb-line structure with transverse electro-magnetic (TEM) mode resonators [3], [4]. Dielectric resonators with non-TEM modes were later used to build waveguide MDR filters [5]–[7]. A dielectric rod with one end short-circuited was used to form an MDR filter supporting TM_{01} mode [8]. Very recently, a dielectric rectangular waveguide resonator loaded by a metalized cylindrical ridge is presented in [9] for supporting a quasi-TEM mode. The cylindrical ridge, or blind hole, on top of the resonator, can reduce the size of the resonator as compared with a normal dielectric waveguide resonator and fine-tune the resonating frequency, bringing great flexibility in coupling layout. With its relatively high unloaded Q factor and compact volume, such kinds of MDR filters have been widely adopted in 5G wireless systems.

The most convenient way to realize TZs in a compact MDR filter is to use cascaded N-tuplet units [10], among which the two simplest cross-coupled units are triplet and quadruplet. A cascaded quadruplet (CQ) unit is favorably used to create two TZs in a four-pole response. However, when the flexibility of TZ control is concerned, a compulsory diagonal cross coupling in the CQ unit must be under control although it may not be feasible in a compact MDR filter.

Dispersion effect inherently exists in coupling elements of a quasi-TEM mode MDR filter. A coupling element on the shortest signal path with strong dispersion can be used to generate a TZ when the element resonates near the passband [11]–[14]. Recently, various efforts have been devoted to synthesize bandpass filters with dispersive coupling elements for creating TZs [15]–[19]. In fact, another application of dispersive coupling elements is to control the sign of coupling in a relatively simple manner. The principle is that when the resonant frequency of the dispersive coupling element situates far away from the passband, its coupling value is either positive or negative depending on which side of the passband the resonance occurs. Such a coupling value varies with frequency monotonically, exhibiting a dispersion effect. In using such a dispersive coupling element in a quasi-TEM mode MDR filter, extra caution is required to ensure the spurious resonance is far enough from the passband.

In practice, dispersive couplings can also appear on a nonshortest signal path in a cascaded unit. The synthesis of such a filter is first presented in [20], in which a dispersive filter in the folded form is addressed. Most recently, a systematic synthesis of bandpass filters with more useful dispersive coupling units, i.e., duplets, triplets, and quadruplets,

Manuscript received June 26, 2021; revised October 7, 2021 and January 25, 2022; accepted March 20, 2022. Date of publication April 11, 2022; date of current version June 3, 2022. This work was supported by Huawei Technologies Company Ltd. *(Corresponding author: Ke-Li Wu.)*

The authors are with the Department of Electronic Engineering, The Chinese University of Hong Kong, Hong Kong (e-mail: yzhang@link.cuhk.edu.hk; ylchen@link.cuhk.edu.hk; klwu@cuhk.edu.hk).

Color versions of one or more figures in this article are available at https://doi.org/10.1109/TMTT.2022.3162872.

Digital Object Identifier 10.1109/TMTT.2022.3162872

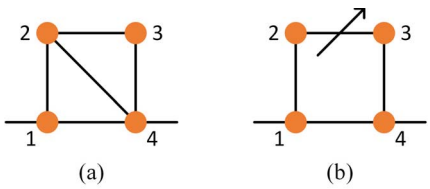

Fig. 1. (a) Dispersion-less quadruplet with a diagonal cross coupling. (b) Quadruplet with a dispersive coupling element on the nonshortest path, where the arrow denotes a dispersive coupling.

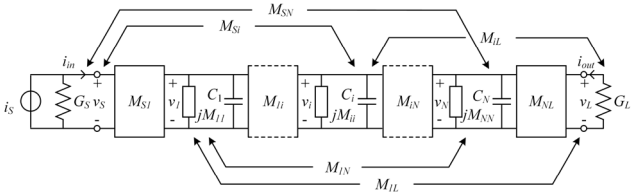

Fig. 2. Low-pass prototype of a coupled resonator network.

is reported [21]. It is shown that a dispersive coupling that is not on the shortest path in a quadruplet can play the role of diagonal cross coupling. In another word, the quadruplet unit shown in Fig. 1(a) can be realized by the quadruplet unit in Fig. 1(b), where the diagonal cross coupling is absorbed into the dispersive coupling element. For the sake of simplicity, the dispersive coupling always refers to the coupling between resonators 2 and 3 when it is mentioned in a quadruplet in this article.

Theoretically, the rejection rate near the passband is traded off by controlling the locations of the two TZs. When a CQ unit is involved, accurate control of the diagonal cross coupling would be very important in filter design. However, due to the inevitable dispersion and the integrality feature of an MDR filter, it is difficult to control the diagonal cross coupling in a physical realization.

To realize a negative coupling in CQs in MDR filters with the quasi-TEM mode, a metalized blind hole between two ridge-loaded waveguide resonators is a good choice with the merit of manufacturing convenience [9]. However, the blind hole is a dispersive coupling element, whose dispersion effect needs to be taken into consideration in the filter synthesis and design. In contrast, a positive coupling is conventionally realized by a partitioning wall formed by a vertical channel in one or two sides of the dielectric block.

It is known that the quadruplet unit in Fig. 1(a) can realize all the three possible responses with two TZs: 1) the two TZs locate on the right-hand side of the passband when all couplings are of the same sign; 2) the two TZs locate on the left-hand side of the passband when M_{24} is with the opposite sign as that of the rest of couplings; and 3) one TZ is on each side of the passband when M_{14} or M_{23} is with the opposite sign as that of the rest of couplings except M_{24}. In the last scenario, the lower (higher) TZ is closer to the passband if the diagonal cross coupling M_{24} is with the opposite (same) sign as that of M_{23} when all the other sequential couplings are positive. The response becomes symmetric when the diagonal cross coupling vanishes.

This article will focus on a novel physical realization of a quadruplet for MDR filters using quasi-TEM mode resonators. The structure can provide an accurate control of TZs on each side of the passband without using a diagonal cross coupling element and is highly suitable for the stamping press manufacturing process. With the structure, the traditional center partitioning walls for positive couplings are replaced by metalized through holes, which not only play the role to control a positive coupling but also can adjust the aggregated diagonal cross coupling in a shared cavity where quadruplet resonators dwell. Through a closed-form transformation between the general dispersion-less coupling matrix of a CQ unit to its dispersive counterpart, it can be mathematically justified that adjusting the diagonal cross coupling equivalently controls the dispersion effect of the dispersive coupling element to achieve various symmetric and asymmetric responses. A design example of a quadruplet MDR filter with two symmetric TZs is given to illustrate how to use the transformation to guide the design. A practical eight-pole MDR filter is designed and prototyped using the proposed structure. The excellent rejection response justifies the effectiveness of the proposed structure and demonstrates the usefulness of the quadruplet structure in an MDR filter when the rejection specifications near the passband are stringent.

II. Theory

A. Congruence Transformation of Coupling Matrix

The loop equation for a dispersion-less coupled resonator network in the low-pass domain, as shown in Fig. 2, can be expressed as

$$\begin{bmatrix} i_S \\ 0 \\ \vdots \\ 0 \\ 0 \end{bmatrix} = \left(\left[\begin{array}{c|c} \mathbf{G} & \mathbf{0} \\ \hline \mathbf{0} & \mathbf{0} \end{array}\right] + j \left[\begin{array}{c|c} \mathbf{0} & \mathbf{B}^T \\ \hline \mathbf{B} & \mathbf{M} \end{array}\right] + s \left[\begin{array}{c|c} \mathbf{0} & \mathbf{0} \\ \hline \mathbf{0} & \mathbf{I} \end{array}\right] \right) \begin{bmatrix} v_S \\ v_L \\ v_1 \\ \vdots \\ v_N \end{bmatrix} \tag{1}$$

where the port admittance matrix $\mathbf{G}$ is a 2×2 diagonal matrix with entries of G_S and G_L, the $N \times N$ identity matrix $\mathbf{I}$ states that all the capacitance C_i $(i = 1, \ldots, N)$ are scaled to 1 [1], $\mathbf{B}$ is an $N \times 2$ matrix whose entries are the couplings between input/output (I/O) and resonators, $\mathbf{M}$ is an $N \times N$ matrix consisting of couplings between resonators and diagonal self-couplings, and $s = j\omega$ with ω being the low-pass frequency.

Since $i_{\text{in}} = i_S - G_S v_S$ and $i_{\text{out}} = -G_L v_L$

$$\begin{bmatrix} i_{\text{in}} \\ i_{\text{out}} \end{bmatrix} = j\mathbf{B}^T \begin{bmatrix} v_1 \\ \vdots \\ v_N \end{bmatrix} \tag{2}$$

assuming there is no direct coupling between source and load. Consider that $v_{\text{in}} = v_S$, $v_{\text{out}} = v_L$, it can be found that

$$\begin{bmatrix} v_1 \\ \vdots \\ v_N \end{bmatrix} = -(j\mathbf{M} + s\mathbf{I})^{-1} j\mathbf{B} \begin{bmatrix} v_{\text{in}} \\ v_{\text{out}} \end{bmatrix}. \tag{3}$$

Substituting the node voltage vector in (3) into (2) results in

$$\begin{bmatrix} i_{\text{in}} \\ i_{\text{out}} \end{bmatrix} = -j\mathbf{B}^T(\mathbf{M}+\omega\mathbf{I})^{-1}\mathbf{B}\begin{bmatrix} v_{\text{in}} \\ v_{\text{out}} \end{bmatrix} \tag{4}$$

from which the admittance matrix related to port voltages and currents can be written as

$$\begin{aligned}\mathbf{Y} &= -j\mathbf{B}^T(\mathbf{M}+\omega\mathbf{I})^{-1}\mathbf{B} \\ &= -j\mathbf{B}^T\boldsymbol{\Sigma}(\boldsymbol{\Sigma}\mathbf{M}\boldsymbol{\Sigma}+\omega\boldsymbol{\Sigma}\boldsymbol{\Sigma})^{-1}\boldsymbol{\Sigma}\mathbf{B} \\ &= -j\mathbf{B}^T\boldsymbol{\Sigma}\mathbf{P}^T\left(\mathbf{P}\boldsymbol{\Sigma}\mathbf{M}\boldsymbol{\Sigma}\mathbf{P}^T+\omega\mathbf{P}\boldsymbol{\Sigma}\boldsymbol{\Sigma}\mathbf{P}^T\right)^{-1}\mathbf{P}\boldsymbol{\Sigma}\mathbf{B} \\ &= -j\mathbf{B}'^T(\mathbf{M}_0+\omega\mathbf{M}_d)^{-1}\mathbf{B}'\end{aligned} \tag{5}$$

where $\boldsymbol{\Sigma}$ and $\mathbf{P}$ are diagonal matrix and orthogonal matrix, respectively, with rank $(\boldsymbol{\Sigma}) = N$. The development of (5) states that a dispersion-less coupled resonator network can be equivalently represented by a dispersive coupling matrix with its value at the center frequency $\mathbf{M}_0 = \mathbf{P}\boldsymbol{\Sigma}\mathbf{M}\boldsymbol{\Sigma}\mathbf{P}^T$, the dispersion slope matrix $\mathbf{M}_d = \mathbf{P}\boldsymbol{\Sigma}\boldsymbol{\Sigma}\mathbf{P}^T$ that is with unity diagonal entries and nonzero entries at the designated location(s), and the constant matrix $\mathbf{B}' = \mathbf{P}\boldsymbol{\Sigma}\mathbf{B}$ that presents coupling between I/O and resonators if there is any.

By setting $\mathbf{Q} = \mathbf{P}\boldsymbol{\Sigma}$, the dispersive coupling matrix $\mathbf{M}(\omega) = \mathbf{M}_0 + \mathbf{M}_d\ \omega$, and $\mathbf{B}' = \mathbf{Q}\mathbf{B}$, where

$$\mathbf{M}_0 = \mathbf{Q}\mathbf{M}\mathbf{Q}^T \tag{6}$$

$$\mathbf{M}_d = \mathbf{Q}\mathbf{Q}^T. \tag{7}$$

Having said that conducting the transformation becomes a matter of finding the transformation matrix $\mathbf{Q}$ subject to solving a set of polynomial equations that are established based on the designated coupling topology and the assignment of dispersive coupling elements such that [22]

$$\begin{aligned}(\mathbf{Q}\mathbf{B})_{i,j} &= 0, \quad \text{for } (i,j) \in T_1 \\ \left(\mathbf{Q}\mathbf{M}\mathbf{Q}^T\right)_{i,j} &= 0, \quad \text{for } (i,j) \in T_2 \\ \left(\mathbf{Q}\mathbf{Q}^T\right)_{i,j} &= 0, \quad \text{for } (i,j) \in T_3 \\ \left(\mathbf{Q}\mathbf{Q}^T\right)_{i,i} - 1 &= 0, \quad \text{for } i = 1,\ldots,N\end{aligned} \tag{8}$$

where T_1, T_2, and T_3 are the sets of indices of the couplings that are supposed to be zero between: 1) I/O and resonators; 2) uncoupled resonators; and 3) dispersion-less couplings, respectively.

B. Transformation for the Quadruplet

In this section, the direct transformation to convert the dispersion-less quadruplet unit shown in Fig. 1(a) into the dispersive quadruplet unit shown in Fig. 1(b) is established. Let $\mathbf{M}$ be the dispersion-less coupling matrix of the dispersion-less quadruplet and $\mathbf{Q}$ be the unknown transformation matrix defined in (6) and (7), whose solution leads to $\mathbf{M}_0$ and $\mathbf{M}_d$ with the designated coupling topology shown in Fig. 1(b).

Referring to Fig. 1(b), the specific sets of null coupling indices for applying (8) can be set as

$$\begin{aligned}T_1 &= \{(S,2),(S,3),(S,4),(L,1),(L,2),(L,3)\} \\ T_2 &= \{(1,3)\} \\ T_3 &= \{(1,2),(1,3),(1,4),(2,4),(3,4)\}.\end{aligned}$$

By neglecting the trivial solutions due to sign symmetries, the unique solution of the matrix $\mathbf{Q}$ can be analytically found as

$$\mathbf{Q} = \begin{pmatrix} 1 & 0 & 0 & 0 \\ 0 & \dfrac{M_{34}}{\sqrt{M_{24}^2+M_{34}^2}} & \dfrac{-M_{24}}{\sqrt{M_{24}^2+M_{34}^2}} & 0 \\ 0 & 0 & 1 & 0 \\ 0 & 0 & 0 & 1 \end{pmatrix}. \tag{9}$$

Substituting the matrix $\mathbf{Q}$ into (6) and (7) leads to the dispersive coupling matrix corresponding to the topology in Fig. 1(b)

$$\begin{aligned}&M_0(1,1) = M_{11},\ M_0(3,3) = M_{33},\ M_0(4,4) = M_{44}, \\ &M_0(3,4) = M_{34},\ M_0(1,4) = M_{14},\ M_0(1,2) = \frac{M_{12}M_{34}}{\sqrt{M_{24}^2+M_{34}^2}} \\ &M_0(2,2) = \frac{M_{33}M_{24}^2 - 2M_{23}M_{24}M_{34} + M_{22}M_{34}^2}{M_{24}^2+M_{34}^2} \\ &M_0(2,3) = \frac{M_{23}M_{34} - M_{24}M_{33}}{\sqrt{M_{24}^2+M_{34}^2}}\end{aligned} \tag{10}$$

and

$$M_d(2,3) = \frac{-M_{24}}{\sqrt{M_{24}^2+M_{34}^2}}. \tag{11}$$

Note that $\mathbf{B}$ remains unchanged after the transformation.

It is clearly stated that M_d (2, 3) exhibits an opposite sign as that of M_{24} and that $M_{24} = 0$ leads to the vanishing of M_d (2, 3).

As mentioned before, for the response with two TZs located at different sides of the passband, the sign of M_{24} decides the relative locations of the TZs. According to (11), the sign of M_d (2, 3) determines the side of the TZ that is closer to the passband. A symmetric response can be realized when M_d (2, 3) = 0. The asymmetry of the two TZs becomes stronger with the increase of the absolute value of M_d (2, 3).

It must be mentioned that due to the complex multiple cross couplings and the dispersion effect, the equivalent circuit shown in Fig. 1(b), although which is not physical, provides a unique and convenient representation of the dispersive CQ unit for filter design and tuning.

III. Proposed Quadruplet Structure

A. Control of Diagonal Cross Coupling

Conventional design of a quadruplet by means of the MDR configuration is shown in Fig. 3(a), in which positive coupling is implemented by a partitioning wall formed by a vertical channel of the dielectric block and the negative coupling M_{23} is realized by a blind metalized hole. The relative permittivity of the dielectric is 19.15. A typical response of the quadruplet with one TZ on each side is shown in Fig. 3(b), in which the center frequency $f_0 = 3.6$ GHz and the bandwidth BW = 0.2 GHz. Although partitioning walls are inserted to physically isolate the cross-coupled resonators, a pair of asymmetric TZs is still seen due to the dispersion effect of the blind hole for negative M_{23}.

To mediate the asymmetry in the response, an appropriate positive diagonal cross coupling M_{24} needs to be introduced.

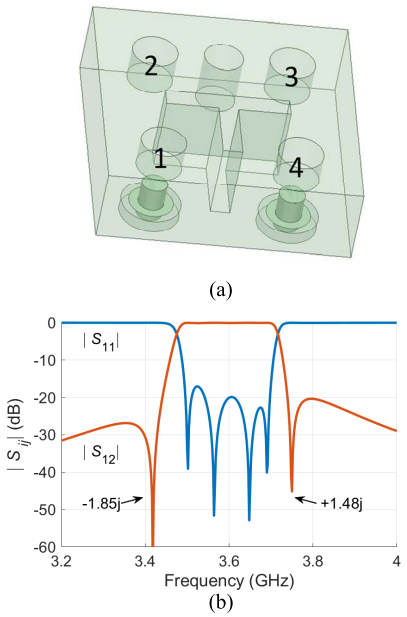

Fig. 3. (a) Layout of conventional quadruplet with a partial-height post placed between resonators 2 and 3 as negative coupling element and partitioning walls as positive coupling elements, and (b) asymmetric response of the MDR quadruplet filter.

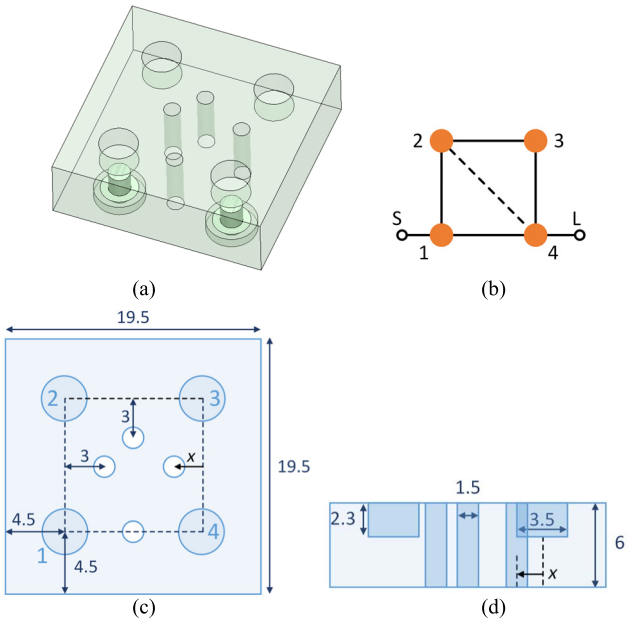

Fig. 4. (a) Structure of an MDR quadruplet with only positive couplings realized by through holes. (b) Corresponding coupling topology of (a) with diagonal parasitic coupling depicted by a dashed line. (c) Top view and (d) front view with typical dimensions of the structure in (a) (unit: mm).

In this article, metalized through holes are used to replace the partitioning wall in the conventional MDR filter design and to compensate the dispersion effect. Fig. 4(a) illustrates one embodiment of the proposed quadruplet structure, showing a shared cavity for four resonators. The through holes are introduced to control the positive sequential coupling in the MDR filter with the quasi-TEM mode while offering an ability to adjust the diagonal cross coupling that occurs in

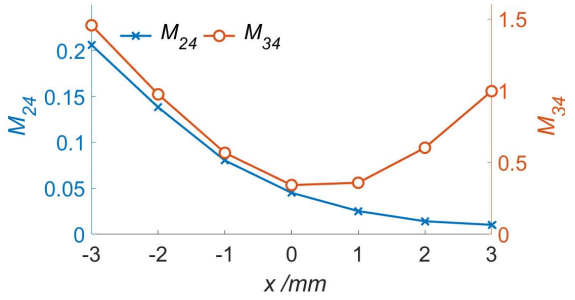

Fig. 5. Diagonal cross coupling M_{24} and the sequential coupling M_{34} versus the offset x. Rest of physical dimensions of the quadruplet are given in Fig. 4.

the shared cavity. Define the offset variable x of a through hole coupling element away from the center-to-center line of the two concerned resonators to be: 1) negative, if the hole is closer to the outside wall; 2) positive, if closer to the center of the cavity; and 3) zero, if on the line. It is found that the offset x affects both the designated positive coupling and the parasitic diagonal cross coupling. Based on the typical dimensions shown in Fig. 4(c) and (d), the joint changes of designated coupling M_{34} and diagonal cross coupling M_{24} by varying the offset x that is associated with M_{34} are depicted in Fig. 5.

By varying the offset x and extracting the coupling matrix corresponding to the topology shown in Fig. 4(b) using the model-based vector fitting (MVF) method [23], it can be observed that only M_{24} and M_{34} change noticeably with the other mutual couplings being stable. As plotted in Fig. 5, when $x = 1$–3 mm (the through hole is close to the center), M_{24} is negligibly small. When the through hole is closer to the outer sidewall (x is a negative value), M_{24} increases monotonously. The through hole acts like a "valve" that controls the leakage of the diagonal cross coupling. The sequential coupling M_{34} becomes minimum when the through hole situates at the center of resonators 3 and 4 and increases as it is moved away from the center-to-center line.

Based on the above-mentioned observation, the diagonal cross coupling can be controlled by shifting the position of the through hole with respect to the center-to-center line. According to (11), this feature equivalently compensates dispersion slope M_d (2, 3).

B. Dispersion Characteristic of the Blind Hole

Another embodiment of the proposed quadruplet structure is shown in Fig. 6(a), where a negative coupling (2, 3) is realized by a blind metalized hole and two through holes are utilized to realize coupling (1, 4) that is much weaker than other mutual couplings. Such a quadruplet generates two TZs, one on each side of the passband. The coupling topology of the quadruplet with the dispersive coupling element can be presented in Fig. 6(b). It will be found that the dispersion property decisively determines the relative locations of the two TZs, whereas the relative locations of the through holes will significantly affect the dispersion slope. Typical dimensions of the CQ unit in the 3.6-GHz frequency band are listed in Fig. 6(c) and (d). Two scenarios are investigated here: the

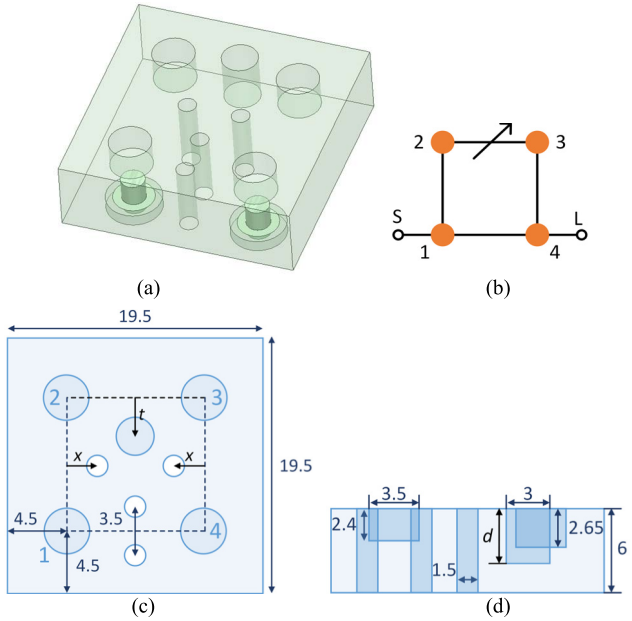

Fig. 6. (a) Structure of an MDR quadruplet with the negative coupling realized by a blind hole between resonators 2 and 3, and other positive couplings realized by through holes. (b) Corresponding coupling topology of (a) with the dispersive coupling depicted by an arrow. (c) The top view and (d) side view with typical dimensions of the structure in (a) (unit: mm).

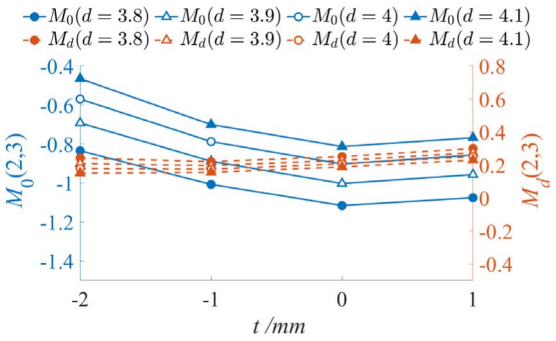

Fig. 7. Constant part M_0 and the slope M_d of the dispersive coupling (2, 3) versus offset t and depth d of the blind hole when $x = 3$ mm.

through holes are moved toward the center (in the case of $x = 3$) and toward the outside walls (in the case of $x = -2$), for which M_0 (2, 3) and M_d (2, 3) are extracted from EM simulation response for different offset distance t of the blind hole from the center-to-center line and depth d of the blind hole.

When the through hole is positioned at $x = 3$, the diagonal cross couplings are blocked according to the previous result. Therefore, the dispersion characteristic of a blind hole can be analyzed as plotted in Fig. 7. The magnitude of M_0 (2, 3) decreases as the blind hole is moved toward the center and reaches the minimum when situating on the center-to-center line. It also decreases as d increases. However, M_d (2, 3) is insensitive to both parameters t and d. It is worth mentioning that although M_d (2, 3) can be increased by decreasing the radius of the blind hole, it is not advisable as it will bring

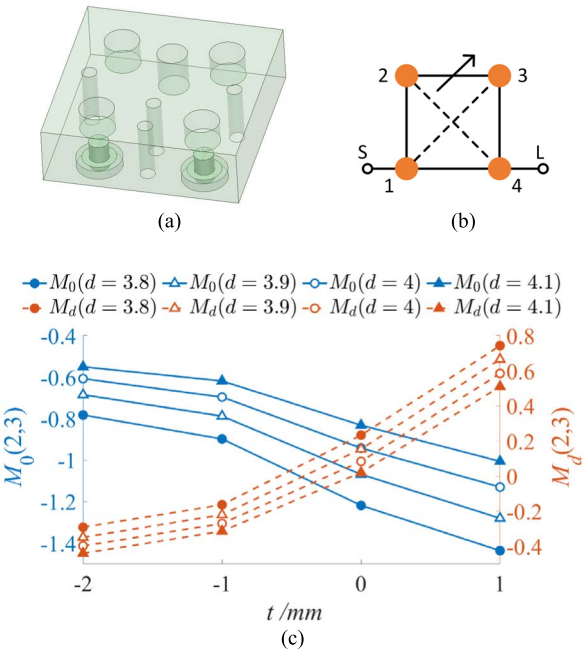

Fig. 8. (a) Structure of the MDR quadruplet in Fig. 6 when $x = -2$ mm. (b) Physical topology of the structure in (a) with the two diagonal cross couplings represented by dashed lines. (c) Constant part M_0 and slope M_d of the dispersive coupling (2, 3) versus offset t and depth d of the blind hole in (a).

the spurious resonance in the lower rejection band closer to the passband.

When $x = -2$ with the representative layout shown in Fig. 8(a), the parasitic diagonal cross coupling is increased as compared with the case of $x = 3$. The coupling topology of this case is shown in Fig. 8(b), where both diagonal couplings and the dispersive coupling exist. To avoid any ambiguity of this multiple solution problem, which is proven in Appendix, the circuit model of Fig. 1(b) is used, by which the diagonal couplings are absorbed into the aggregated dispersive coupling (2, 3). With the existence of the diagonal cross couplings, the aggregated dispersion defined in Fig. 1(b) presents a larger range of realizable values by adjusting the offset t and depth d of the blind hole. As revealed in Fig. 8(c), increasing t will increase M_d (2, 3) and decrease M_0 (2, 3), whereas increasing d leads to opposite changes. Comparing with Fig. 7, both M_d (2, 3) and M_0 (2, 3) can be controlled in a larger range. M_d (2, 3) can vary from a negative value to a positive value. The large variation range of the aggregated dispersive coupling provides a large range of control for the two TZs on different sides of the passband. An attractive feature of this structure is that the spurious mode in the lower rejection band is not affected even when M_d (2, 3) is as large as 0.8. The spurious mode performance is not sacrificed since the nature of the blind hole is not affected.

Having understood the equivalence between the dispersionless and dispersive coupling matrices for the CQ unit, one can vary M_d (2, 3) by managing the diagonal cross coupling M_{24} or vice versa.

To illustrate the concept of compensation, the dispersionless coupling matrix for the response shown in Fig. 3(b) is

extracted using MVF as

$$\mathbf{M}=\begin{pmatrix} 0 & 1.0098 & 0 & 0 & 0 & 0 \\ 1.0098 & 0.0064 & 0.8392 & 0 & 0.2751 & 0 \\ 0 & 0.8392 & 0.1276 & -0.7968 & -0.1513 & 0 \\ 0 & 0 & -0.7968 & -0.1663 & 0.8246 & 0 \\ 0 & 0.2751 & -0.1513 & 0.8246 & 0.0092 & 1.0157 \\ 0 & 0 & 0 & 0 & 1.0157 & 0 \end{pmatrix} \tag{12}$$

whose dispersive counterpart can be obtained by (10) and (11) as

$$\mathbf{M}_0=\begin{pmatrix} 0 & 1.0098 & 0 & 0 & 0 & 0 \\ 1.0098 & 0.0064 & 0.8254 & 0 & 0.2751 & 0 \\ 0 & 0.8254 & -0.1648 & -0.8137 & 0 & 0 \\ 0 & 0 & -0.8137 & -0.1663 & 0.8246 & 0 \\ 0 & 0.2751 & 0 & 0.8246 & 0.0092 & 1.0157 \\ 0 & 0 & 0 & 0 & 1.0157 & 0 \end{pmatrix} \tag{13}$$

with $M_d\ (2, 3) = 0.1805$, which is comparable with the natural dispersion characteristic shown in Fig. 7. As long as $M_d\ (2, 3)$ is positive, the TZ in the higher rejection band will be closer to the passband than the one in the lower rejection band.

To control the TZs of an MDR filter containing a CQ unit, the dispersion slope $M_d\ (2, 3)$ must be under control to a certain extent. However, in most cases, the blind hole coupling structure only provides very limited control to its dispersion slope, e.g., only positive. To accommodate this limitation, the through holes provide a unique way to not only realize the required positive couplings but also introduce a parasitic diagonal cross coupling to compensate the dispersion effect.

IV. Design Examples

In this section, two MDR filters with the proposed dispersive CQ unit will be designed to demonstrate the control of the two TZs: a quadruplet filter with two symmetric TZs and an eight-pole filter containing a CQ for generating a pair of TZs with the lower one closer to the passband and a box unit. Neither of the two responses can be realized by the conventional MDR quadruplet structure in Fig. 3(a).

A. Quadruplet Filter With Two Symmetric TZs

A quadruplet filter with two symmetric TZs is first synthesized based on the topology in Fig. 1(b). The center frequency of the filter $f_0 = 3.6$ GHz and the bandwidth BW $= 0.2$ GHz. For return loss RL $= 20$ dB and two normalized TZs at $\pm 1.73\,j$, the synthesized coupling matrix can be found as

$$\mathbf{M}=\begin{pmatrix} 0 & 1.0196 & 0 & 0 & 0 & 0 \\ 1.0196 & 0 & 0.8488 & 0 & 0.2424 & 0 \\ 0 & 0.8488 & 0 & -0.7946 & 0 & 0 \\ 0 & 0 & -0.7946 & 0 & 0.8488 & 0 \\ 0 & 0.2424 & 0 & 0.8488 & 0 & 1.0196 \\ 0 & 0 & 0 & 0 & 1.0196 & 0 \end{pmatrix} \tag{14}$$

whose dispersive counterpart can be found, through (10) and (11), as $\mathbf{M}_0 = \mathbf{M}$ with $M_d\ (2, 3) = 0$.

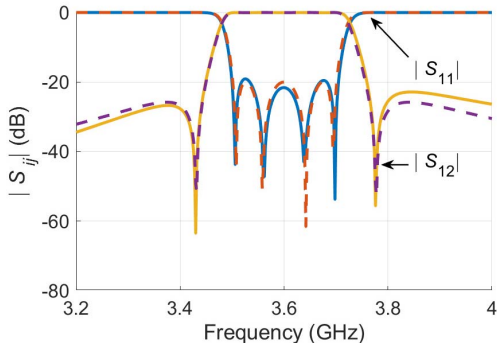

Fig. 9. Responses of the synthesized dispersive coupling matrix (dashed lines) and EM designed model (solid lines) of the quadruplet filter with two symmetric TZs.

TABLE I
Rejection Specifications of the Filter

Frequency range (MHz)	Specification (dB)	Frequency range (MHz)	Specification (dB)
<2437	-58	2437~3049	-70
3049~3197	-35	3197~3338	-71
3338~3479	-40	3761~3881	-40
3881~3952	-45	3952~4044	-40
4044~4609	-25	4609~5137	-56
5137~5883	-25	>5883	-15

The physical realization of this filter looks the same as that in Fig. 6. By comparing the extracted coupling matrix of each EM design step with the synthesized coupling matrix, physical dimensions can be adjusted until the response matches the desired one. The final responses of the EM designed and the synthesized are superposed in Fig. 9, showing good flexibility of the proposed quadruplet structure in TZ control.

B. Eight-Pole Filter With CQ and Box Topology

In this section, an eight-pole MDR filter that contains one CQ unit and one box unit is designed and fabricated to demonstrate the proposed novel CQ structure. It will be demonstrated that the proposed quadruplet structure can be applied to an MDR filter to precisely control the two TZs near the passband. In this case, the lower TZ is closer to the passband than the higher one, which is also unrealizable by the conventional structure in Fig. 3(a).

According to the stringent rejection specifications as listed in Table I, the eight-pole filter with four TZs that are evenly located on both sides of the passband is synthesizedas shown in Fig. 10. The passband is from 3.5 to 3.73 GHz and the four normalized TZs are $-1.93\,j$, $-1.20\,j$, $1.30\,j$, and $2.81\,j$, among which TZs $-1.20\,j$ and $1.30\,j$ are realized by the dispersive CQ unit, whereas TZs $-1.93\,j$ and $2.81\,j$ are realized by the box unit. Notice that the specifications in the lower rejection band are barely met, meaning that the locations of two lower TZs need to be precisely controlled. Even though the specifications in the higher rejection band are not too tight, the two higher

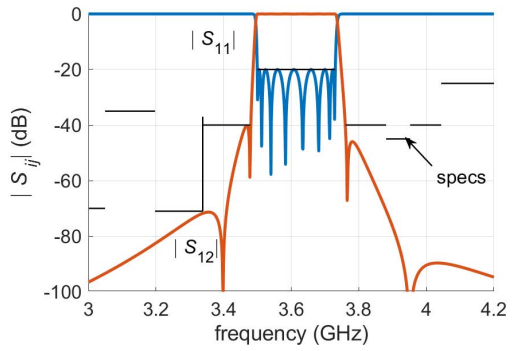

Fig. 10. Synthesized response together with narrowband specifications.

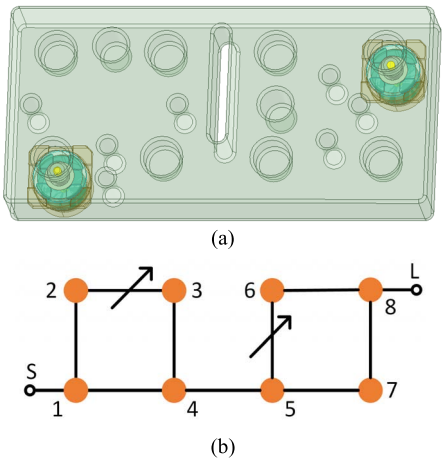

Fig. 11. (a) Model and (b) corresponding topology of the eight-pole MDR filter.

TZs also need to be well controlled since any deviation will affect the response in the lower rejection band. In fact, only the TZ that is farthest from the passband in the higher rejection band can be relaxed a bit.

It is obvious that the synthesized response requires precise control of the diagonal cross coupling since both lower TZs are closer to the passband than the higher TZs. Therefore, the proposed structure will be used to deal with this case. It is straightforward to come up with the topology with two CQs to realize the two pairs of TZs. However, the proposed quadruplet structure forms a shared cavity which produces a spurious mode in the higher rejection band. As the result, when the CQ unit is used in a two cascaded CQ configuration, two spurious modes distinctly appear. To suppress the spurious modes, a four-pole box unit of resonators 5-6-7-8 is cascaded to the CQ unit, as shown in Fig. 11(a), with its coupling topology shown in Fig. 11(b). In this filter structure, the first unit is the CQ with three positive couplings controlled by metalized through holes closer to the outside walls and one negative coupling realized by a blind hole, while the second unit is the box in which three positive couplings are implemented by the through holes closer to the center and one negative coupling is realized by a blind hole. Since the frequencies of the parasitic resonant modes in the two different shared cavities are different, the spurious modes can be suppressed.

In this design, the pair of TZs that are closest to the passband are realized by the CQ unit (1-2-3-4) as they can be well controlled by the proposed CQ structure. The other two TZs are assigned to the box unit. Unlike a traditional four-pole box unit that can only realize one TZ, the dispersive negative coupling M_{56} in the box can generate the farthest TZ in the higher rejection band.

The synthesized coupling matrix is listed at the bottom of the page. The four-pole box has two solutions, but only the one that is convenient to be realized by an MDR filter is used in this design. In practice, a blind hole negative

$$\mathbf{M}_0 = \begin{pmatrix} 0 & 0.9857 & 0 & 0 & 0 & 0 & 0 & 0 & 0 & 0 \\ 0.9857 & -0.0025 & 0.7509 & 0 & 0.2922 & 0 & 0 & 0 & 0 & 0 \\ 0 & 0.7509 & 0.1722 & -0.7777 & 0 & 0 & 0 & 0 & 0 & 0 \\ 0 & 0 & -0.7777 & 0.1332 & 0.4659 & 0 & 0 & 0 & 0 & 0 \\ 0 & 0.2922 & 0 & 0.4659 & -0.0049 & 0.5293 & 0 & 0 & 0 & 0 \\ 0 & 0 & 0 & 0 & 0.5293 & -0.0859 & -0.4547 & 0.3503 & 0 & 0 \\ 0 & 0 & 0 & 0 & 0 & -0.4547 & -0.5658 & 0 & 0.6037 & 0 \\ 0 & 0 & 0 & 0 & 0 & 0.3503 & 0 & 0.6743 & 0.5426 & 0 \\ 0 & 0 & 0 & 0 & 0 & 0 & 0.6037 & 0.5426 & -0.0025 & 0.9857 \\ 0 & 0 & 0 & 0 & 0 & 0 & 0 & 0 & 0.9857 & 0 \end{pmatrix}$$

$$\mathbf{M}_d = \begin{pmatrix} 1 & 0 & 0 & 0 & 0 & 0 & 0 & 0 & 0 & 0 \\ 0 & 1 & 0 & 0 & 0 & 0 & 0 & 0 & 0 & 0 \\ 0 & 0 & 1 & -0.1478 & 0 & 0 & 0 & 0 & 0 & 0 \\ 0 & 0 & -0.1478 & 1 & 0 & 0 & 0 & 0 & 0 & 0 \\ 0 & 0 & 0 & 0 & 1 & 0 & 0 & 0 & 0 & 0 \\ 0 & 0 & 0 & 0 & 0 & 1 & 0.0901 & 0 & 0 & 0 \\ 0 & 0 & 0 & 0 & 0 & 0.0901 & 1 & 0 & 0 & 0 \\ 0 & 0 & 0 & 0 & 0 & 0 & 0 & 1 & 0 & 0 \\ 0 & 0 & 0 & 0 & 0 & 0 & 0 & 0 & 1 & 0 \\ 0 & 0 & 0 & 0 & 0 & 0 & 0 & 0 & 0 & 1 \end{pmatrix}$$

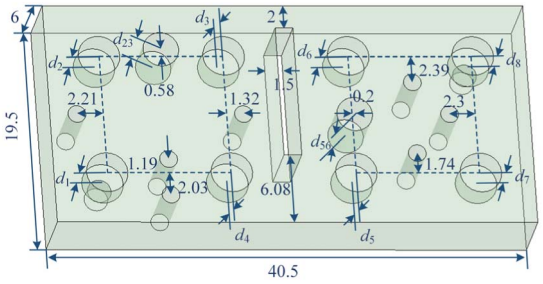

Fig. 12. Dimensions of the simplified simulated model (unit: mm).

TABLE II
DIMENSIONS OF BLIND HOLES IN FIG. 12 (UNIT: mm)

d_1	d_2	d_3	d_4	d_5
2.54	2.732	2.818	2.382	2.596
d_6	d_7	d_8	d_{23}	d_{56}
2.618	2.58	2.504	4.05	4.82

coupling element usually demonstrates a dispersion slope M_d (5,6) $\sim$ 0.09, which is considered in the synthesis stage. However, the proposed CQ structure must be used, in which the parasitic diagonal cross couplings can effectively compensate the dispersion slope of coupling (2, 3) so that the achieved value approaches the synthesized M_d (2, 3) $= -0.1478$.

A simplified model whose fillets and chamfers are not shown is illustrated in Fig. 12 with dimensions listed in Table II to illustrate the key dimensions. The relative permittivity of the dielectric is 19.15 and the loss tangent is 5×10^{-5}. The basic dimensions, such as the radii of the through holes and blind holes, are the same as those in Section III and, therefore, not shown. All of the vertical edges are filleted with a radius of 0.75 mm. The inside edges, or the edges at the bottom of the blind holes, are filleted with a radius of 0.3 mm. The rest of the horizontal edges are chamfered with a distance of 0.3 mm.

The prototyped eight-pole MDR filter is made of a $MgTiO_3$– $CaTiO_3$ based ceramic brick and is manufactured by CNC machining with accuracy of better than $\pm$0.02 mm. The surface silver immersion coating process consists of 2–3 times of immersion, deposition, 200 °C drying, and 800 °C–900 °C baking to plate a 10-μm-thick silver layer on the outer surface. The necessary fine-tuning can be performed by scratching the inner silver-coated surface of the bland holes or through holes. A photograph of the prototyped MDR filter is shown in Fig. 13(a). The measured narrowband and wideband responses are shown in Fig. 13(b) and (c), respectively. It is observed that all of the tight specifications are satisfied. The quality factor of resonators extracted from the measured response is around 1200 and the in-band insertion loss is shown in Fig. 13(b). The spurious mode in the higher rejection band is also successfully suppressed. In the lower frequency band, there are two spurious modes contributed by the two blind holes. It is not an issue as they are sufficiently below the required rejection spec.

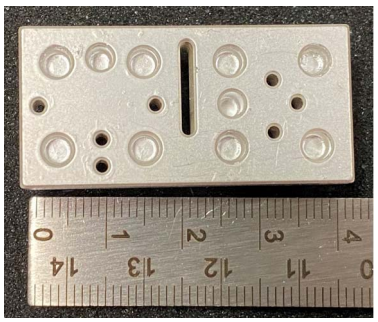

(a)

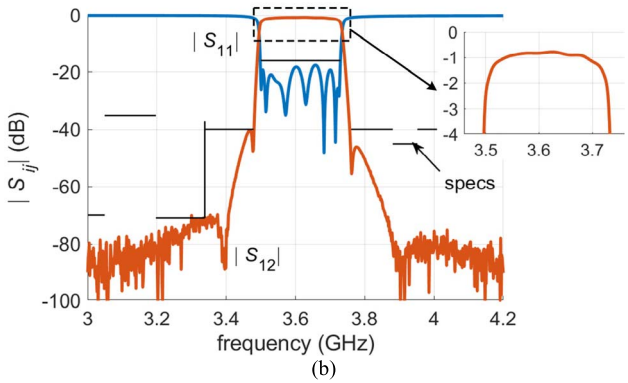

(b)

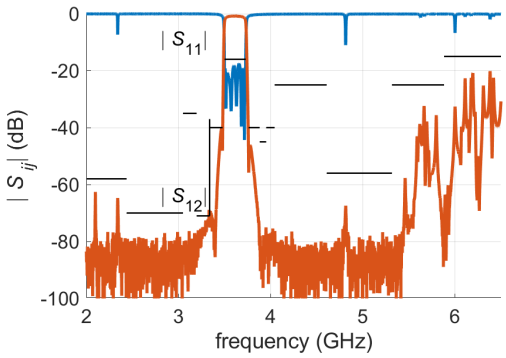

(c)

Fig. 13. (a) Photograph of the prototyped filter. (b) Narrowband and (c) wideband measured response with specifications.

This design example demonstrates the necessity of the proposed CQ structure in designing a high-performance MDR filter when the specifications require stringent control on the TZs. It is also affirmed that a precise compensation of the dispersion slope is very important for accurate control of the TZ pair close to the passband.

V. CONCLUSION

This article concerns an important feature in designing an advanced MDR filter that contains a CQ with a dispersive negative coupling element for realizing two TZs on each side of the passband. A simple-to-make configuration for realizing a coupling controllable CQ is proposed and experimentally validated. It has been demonstrated by EM simulation that by appropriately planting the thin metalized through hole between each pair of sequentially coupled resonators, the dispersion effect caused by the blind hole for negative coupling can be well compensated while controlling

the required positive coupling. Consequently, the TZs of the rejection characteristic near the passband can be very well controlled without introducing extra manufacturing complicity. The closed-form mathematic transformation that reveals the relationship between the diagonal cross coupling and the dispersive negative coupling is developed, which explains the working principle of the proposed CQ structure and provides a design guideline. A design example of a quadruplet MDR filter containing a pair of symmetric TZs is given to illustrate the possibility of compensating the dispersive effect using parasitic couplings. An eight-pole MDR filter that contains one CQ and one box coupling unit is designed and fabricated to demonstrate the proposed structure. Excellent near-passband rejection and spurious resonance suppression can be observed. The proposed CQ structure is especially useful for designing MDR filters where specifications require stringent control on the TZs of the rejections.

Being a relatively new filter format with high potential in M-MIMO base station applications, the MDR filter should receive more attention from academia and industry. Due to the limited space, the details of the dispersive box unit are not discussed. A separate article from the authors will be dedicated to the investigation of dispersive box units in MDR filters in the near future.

APPENDIX

A proof of the infinite number of multiple solutions of the circuit shown in Fig. 8(b) is provided here. Note that the solutions caused by sign symmetries are not considered.

The coupling problem of the dispersive CQ unit described by the circuit shown in Fig. 8(b) can be represented by the following dispersive coupling matrix ($\mathbf{M}_0$, $\mathbf{M}_d$, $\mathbf{B}$):

$$\mathbf{M}_0 = \begin{pmatrix} M_0(1,1) & M_0(1,2) & M_0(1,3) & M_0(1,4) \\ M_0(1,2) & M_0(2,2) & M_0(2,3) & M_0(2,4) \\ M_0(1,3) & M_0(2,3) & M_0(3,3) & M_0(3,4) \\ M_0(1,4) & M_0(2,4) & M_0(3,4) & M_0(4,4) \end{pmatrix} \tag{A1a}$$

$$\mathbf{M}_d = \begin{pmatrix} 1 & 0 & 0 & 0 \\ 0 & 1 & M_d(2,3) & 0 \\ 0 & M_d(2,3) & 1 & 0 \\ 0 & 0 & 0 & 1 \end{pmatrix} \tag{A1b}$$

$$\mathbf{B} = \begin{pmatrix} M(S,1) & 0 & 0 & 0 \\ 0 & 0 & 0 & M(4,L) \end{pmatrix}^T. \tag{A1c}$$

According to (1) through (7), performing the congruence transformation with transformation matrix

$$\mathbf{Q} = \begin{pmatrix} 1 & 0 & 0 & 0 \\ 0 & x_1 & x_2 & 0 \\ 0 & x_3 & x_4 & 0 \\ 0 & 0 & 0 & 1 \end{pmatrix} \tag{A2}$$

will not change the response of the coupled resonator network.

By enforcing resultant M_d (2,2) and M_d (3,3) to be unity after the transformation, the general solution for $\mathbf{Q}$ can be found as

$$x_2 = -M_d(2,3)x_1 - \sqrt{M_d(2,3)^2 x_1^2 - x_1^2 + 1} \tag{A3a}$$

$$x_4 = \sqrt{M_d(2,3)^2 x_3^2 - x_3^2 + 1} - M_d(2,3)x_3 \tag{A3b}$$

where the other two unknowns x_1 and x_3 can be of any values as long as $\mathbf{Q}$ is nonsingular. It justifies that there are infinite number of solutions for the circuit in Fig. 8(b).

By enforcing resultant M_0 (1,3) and M_0 (2,4) to be zero after the transformation, the variables x_1 and x_3 are stipulated by

$$x_1 = \frac{M_0(3,4)}{\sqrt{M_0(2,4)^2 - 2M_d(2,3)M_0(2,4)M_0(3,4) + M_0(3,4)^2}} \tag{A4a}$$

$$x_3 = \frac{M_0(1,3)}{\sqrt{M_0(1,2)^2 - 2M_d(2,3)M_0(1,2)M_0(1,3) + M_0(1,3)^2}} \tag{A4b}$$

which means that the circuit in Fig. 1(b) is with a unique solution. Be noted that the dispersive coupling matrix ($\mathbf{M}_0$, $\mathbf{M}_d$, $\mathbf{B}$) that appeared on the right-hand side of (A3) and (A4) is physical variables, although difficult to acquire.

ACKNOWLEDGMENT

The authors would like to thank Huawei Technologies Company Ltd. for sponsoring this research and Ms. Hua-Hong Wang of Huawei Technologies Co., Ltd. Shenzhen, Guangdong, China. For many useful suggestions and discussions throughout this research and fabricating the prototype filter in this article. They would also like to thank all the reviewers of this article for their valuable comments and suggestions.

REFERENCES

[1] R. J. Cameron, C. M. Kudsia, and R. Mansour, *Microwave Filters for Communication Systems: Fundamentals Design and Applications*, 2nd ed. Hoboken, NJ, USA: Wiley, 2018.

[2] S. Amari and G. Macchiarella, "Synthesis of inline filters with arbitrarily placed attenuation poles by using nonresonating nodes," *IEEE Trans. Microw. Theory Techn.*, vol. 53, no. 10, pp. 3075–3081, Oct. 2005.

[3] R. L. Sokola and C. Choi, "Ceramic bandpass filter," U.S. Patent 4 431 977, Feb. 14, 1984.

[4] D. M. DeMuro and D. Agahi-Kesheh, "Monolithic ceramic filter with bandstop function," U.S. Patent 4 823 098, Apr. 18, 1989.

[5] Y. Konishi, "Novel dielectric waveguide components-microwave applications of new ceramic materials," *Proc. IEEE*, vol. 79, no. 6, pp. 726–740, Jun. 1991.

[6] K. Sano and M. Miyashita, "Dielectric waveguide filter with low profile and low-insertion loss," *IEEE Trans. Microw. Theory Techn.*, vol. 47, no. 12, pp. 2299–2303, Dec. 1999.

[7] I. C. Hunter and M. Y. Sandhu, "Monolithic integrated ceramic waveguide filters," in *IEEE MTT-S Int. Microw. Symp. Dig.*, Jun. 2014, pp. 1–3.

[8] X. Wang and K.-L. Wu, "A TM_{01} mode monoblock dielectric filter," *IEEE Trans. Microw. Theory Techn.*, vol. 62, no. 2, pp. 275–281, Feb. 2014.

[9] B. Yuan, "Filter and transceiver comprising dielectric body resonators having frequency adjusting holes and negative coupling holes," U.S. Patent 9 998 163 B2, Jun. 12, 2018.

[10] S. Tamiazzo and G. Macchiarella, "An analytical technique for the synthesis of cascaded N-tuplets cross-coupled resonators microwave filters using matrix rotations," *IEEE Trans. Microw. Theory Techn.*, vol. 53, no. 5, pp. 1693–1698, May 2005.

[11] M. Ohira, Z. Ma, H. Deguchi, and M. Tsuji, "A novel coaxial-excited FSS-loaded waveguide filter with multiple transmission zeros," in *Proc. Asia–Pacific Microw. Conf.*, Dec. 2010, pp. 1720–1723.

[12] M. Politi and A. Fossati, "Direct coupled waveguide filters with generalized Chebyshev response by resonating coupling structures," in *Proc. Eur. Microw. Conf. (EuMC)*, Sep. 2010, pp. 966–969.

[13] U. Rosenberg and S. Amari, "A novel band-reject element for pseudoelliptic bandstop filters," *IEEE Trans. Microw. Theory Techn.*, vol. 55, no. 4, pp. 742–746, Apr. 2007.

[14] U. Rosenberg, S. Amari, and F. Seyfert, "Pseudo-elliptic direct-coupled resonator filters based on transmission-zero-generating irises," in *Eur. Microw. Conf. Dig.*, Sep. 2010, pp. 962–965.

[15] L. Szydlowski, N. Leszczynska, and M. Mrozowski, "Dimensional synthesis of coupled-resonator pseudoelliptic microwave bandpass filters with constant and dispersive couplings," *IEEE Trans. Microw. Theory Techn.*, vol. 62, no. 8, pp. 1634–1646, Aug. 2014.
[16] L. Szydlowski, A. Lamecki, and M. Mrozowski, "A novel coupling matrix synthesis technique for generalized Chebyshev filters with resonant source–load connection," *IEEE Trans. Microw. Theory Techn.*, vol. 61, no. 10, pp. 3568–3577, Oct. 2013.
[17] L. Szydlowski, N. Leszczynska, and M. Mrozowski, "Generalized Chebyshev bandpass filters with frequency-dependent couplings based on stubs," *IEEE Trans. Microw. Theory Techn.*, vol. 61, no. 10, pp. 3601–3612, Oct. 2013.
[18] Y. He *et al.*, "A direct matrix synthesis for in-line filters with transmission zeros generated by frequency-variant couplings," *IEEE Trans. Microw. Theory Techn.*, vol. 66, no. 4, pp. 1780–1789, May 2018.
[19] Y. Zhang, H. Meng, and K.-L. Wu, "Direct synthesis and design of dispersive waveguide bandpass filters," *IEEE Trans. Microw. Theory Techn.*, vol. 68, no. 5, pp. 1678–1687, May 2020.
[20] S. Tamiazzo and G. Macchiarella, "Synthesis of cross-coupled filters with frequency-dependent couplings," *IEEE Trans. Microw. Theory Techn.*, vol. 65, no. 3, pp. 775–782, Mar. 2017.
[21] Y. Zhang, F. Seyfert, S. Amari, M. Olivi, and K.-L. Wu, "General synthesis method for dispersively coupled resonator filters with cascaded topologies," *IEEE Trans. Microw. Theory Techn.*, vol. 69, no. 2, pp. 1378–1393, Feb. 2021.
[22] R. J. Cameron, J.-C. Faugere, F. Rouillier, and F. Seyfert, "Exhaustive approach to the coupling matrix synthesis problem and application to the design of high degree asymmetric filters," *Int. J. RF Microw. Comput.-Aided Eng.*, vol. 17, no. 1, pp. 4–12, Jan. 2007.
[23] P. Zhao and K.-L. Wu, "Model-based vector-fitting method for circuit model extraction of coupled-resonator diplexers," *IEEE Trans. Microw. Theory Techn.*, vol. 64, no. 6, pp. 1787–1797, Jun. 2016.

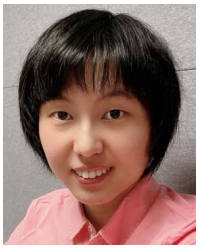

Yan Zhang received the B.S. degree in electronic engineering from the University of Electronic Science and Technology of China, Chengdu, China, in 2017, and the Ph.D. degree from The Chinese University of Hong Kong, Hong Kong, in 2022.

Her current research interests include synthesis and tuning of filters with dispersive couplings and filters with irregular topologies.

Yuliang Chen (Graduate Student Member, IEEE) received the B.Eng. degree in electromagnetic field and wireless technology from Northwestern Polytechnical University, Xi'an, China, in 2017. He is currently pursuing the Ph.D. degree at the Department of Electronic Engineering, The Chinese University of Hong Kong, Hong Kong, SAR, China.

His current research interests include miniaturization techniques and robot automatic tuning of microwave filters for wireless communication.

Ke-Li Wu (Fellow, IEEE) received the B.S. and M.Eng. degrees from Nanjing University of Science and Technology, Nanjing, China, in 1982 and 1985, respectively, and the Ph.D. degree from Laval University, Quebec, QC, Canada, in 1989.

From 1989 to 1993, he was a Research Engineer with McMaster University, Hamilton, ON, Canada. He joined COM DEV (now Honeywell Aerospace), Cambridge, ON, Canada, in 1993, where he was a Principal Member of Technical Staff. Since 1999, he has been with The Chinese University of Hong Kong, Hong Kong, where he is currently a Professor and the Director of the Radio frequency Radiation Research Laboratory. His current research interests include EM-based circuit domain modeling of high-speed interconnections, robot automatic tuning of microwave filters, decoupling techniques of MIMO antennas, and the IoT technologies.

Prof. Wu is also a member of the IEEE MTT-8 Subcommittee. He was a recipient of the 1998 COM DEV Achievement Award and the Asia-Pacific Microwave Conference Prize twice in 2008 and 2012, respectively. He was an Associate Editor of the IEEE TRANSACTIONS ON MICROWAVE THEORY AND TECHNIQUES (MTT) from 2006 to 2009.